Publ. Astron. Soc. Japan 36, 741–759 (1984)

Energy Spectra of Low-Mass Binary X-Ray Sources Observed from Tenma

Kazuhisa MITSUDA, Hajime INOUE, Katsuji KOYAMA, Kazuo MAKISHIMA, Masaru MATSUOKA, Yoshiaki OGAWARA, Noriaki SHIBAZAKI,* Kazuaki SUZUKI, and Yasuo TANAKA

Institute of Space and Astronautical Science, 6-1, Komaba 4-chome, Meguro-ku, Tokyo 153

and

Tatsumi HIRANO

Department of Astrophysics, Faculty of Science, Nagoya University, Furo-cho, Chikusa-ku, Nagoya 464

(Received 1984 May 31; accepted 1984 October 1)

Abstract

Observations of X-ray spectra for four low-mass binary X-ray sources, Sco X-1, 4U 1608−522, GX 5−1, and GX 349+2 were performed with the gas scintillation proportional counters on board Tenma. Common to the four sources, the spectrum hardens with increasing intensity, and the difference of the spectra before and after an intensity increase shows invariably a blackbody spectrum of $kT \cong 2$ keV. Every observed spectrum can be expressed by a sum of two spectral components: a hard component and a soft component, whose spectral shapes are fixed for each individual source. The hard component has a blackbody spectrum of $kT \cong 2$ keV and its intensity varies largely with time. The soft component is best represented by a superposition of multicolor blackbody spectra expected from an optically-thick accretion disk, and its intensity remains faily stable. The spectral shapes of the both components are respectively similar to each other among the four sources, except for different bolometric flux ratio of the two components for the individual sources. The energy spectrum during the transient dips observed from GX 5−1 is in good agreement with that of the soft component, indicating that the 2-keV blackbody component has become almost absent. The 2-keV blackbody component and the soft component may be attributed to the emission from the neutron star surface and that from the optically thick accretion disk, respectively.

Key words: Accretion disks; Neutron stars; X-ray binaries; X-ray sources; X-ray spectra.

* Present address: Department of Physics, University of Illinois, U. S. A.

1. Introduction

Nonpulsating low-mass binary X-ray sources generally have soft X-ray spectra which are roughly approximated by a thin thermal bremsstrahlung spectrum with temperature ranging from 3 to 15 keV. They commonly show irregular intensity variations by a factor of as large as three on time scales of a few tens of minutes to hours. In such variations, a positive correlation between the X-ray spectral hardness and the X-ray intensity is observed from many sources at least on some occasions (Mason et al. 1976; Parsignault and Grindlay 1978; Branduardi et al. 1980; White et al. 1980; Ponman 1982; Oda 1984). So far no satisfactory explanation has been given for this correlation.

Detailed studies of the X-ray spectrum of Sco X-1, a prototype of the low-mass binary X-ray sources, revealed that thin thermal emission spectrum cannot explain the observed spectrum (Laros and Singer 1976; Long and Kestenbaum 1978; Lamb and Sanford 1979). Instead, it was found to be consistent with a Comptonized thermal bremsstrahlung (Felten and Rees 1972; Chapline and Stevens 1973; Miyamoto 1978) from a plasma with a radius of $\sim 10^9$ cm, a temperature of ~ 3 keV and an optical depth of the electron scattering of ~ 20 (e. g., Miyamoto and Matsuoka 1977). However this model seems to be unlikely, because the energy conversion from the neutron star to the hot plasma seems to be difficult. The rapid intensity variations of less than 1 s observed from some low-mass binary X-ray sources (Hoffman et al. 1979) also present difficulty for this model. Similarly for other low-mass binary sources, the nature of the energy spectrum is not well understood.

In this paper, we present an interpretation of new observational results on the X-ray spectra and their temporal variations for four bright low-mass binary X-ray sources. The results are discussed in the context of the disk accretion onto a weakly magnetized neutron star.

2. Observations

We observed four low-mass binary X-ray sources, Sco X-1, 4U 1608−522, GX 5−1, and GX 349+2 with a set of eight gas scintillation proportional counters on board Tenma. The total effective area is 640 cm^2 and the energy resolution is 9.5% FWHM at 5.9 keV. X-rays of energies up to 37 keV are analyzed into 128 pulse-height channels. Details of the instrument are given in separate papers (Tanaka et al. 1984; Koyama et al. 1984). The periods of the observations are listed in table 1. During the observations, attitude of the spacecraft was maintained so as to avoid contaminations from nearby sources. The contamination levels are estimated to be always less than 2% of the total counting rate for each

Table 1. Period of observations.

Source	Date and time (UT)*						
Sco X-1†	1983	April	25	23 h–	April	26	1 h
	1983	April	26	15 h–	April	26	23 h
	1983	April	26	23 h–	April	28	21 h
4U 1608−522	1983	April	20	21 h–	April	22	9 h
GX 349+2	1983	July	28	0 h–	July	29	9 h
	1983	August	1	1 h–	August	4	1 h
GX 5−1	1983	August	22	4 h–	August	24	19 h

* The total observation time is effectively 5 hours per day.

† Observational data on April 26, 15–23 UT were used in the present analyses.

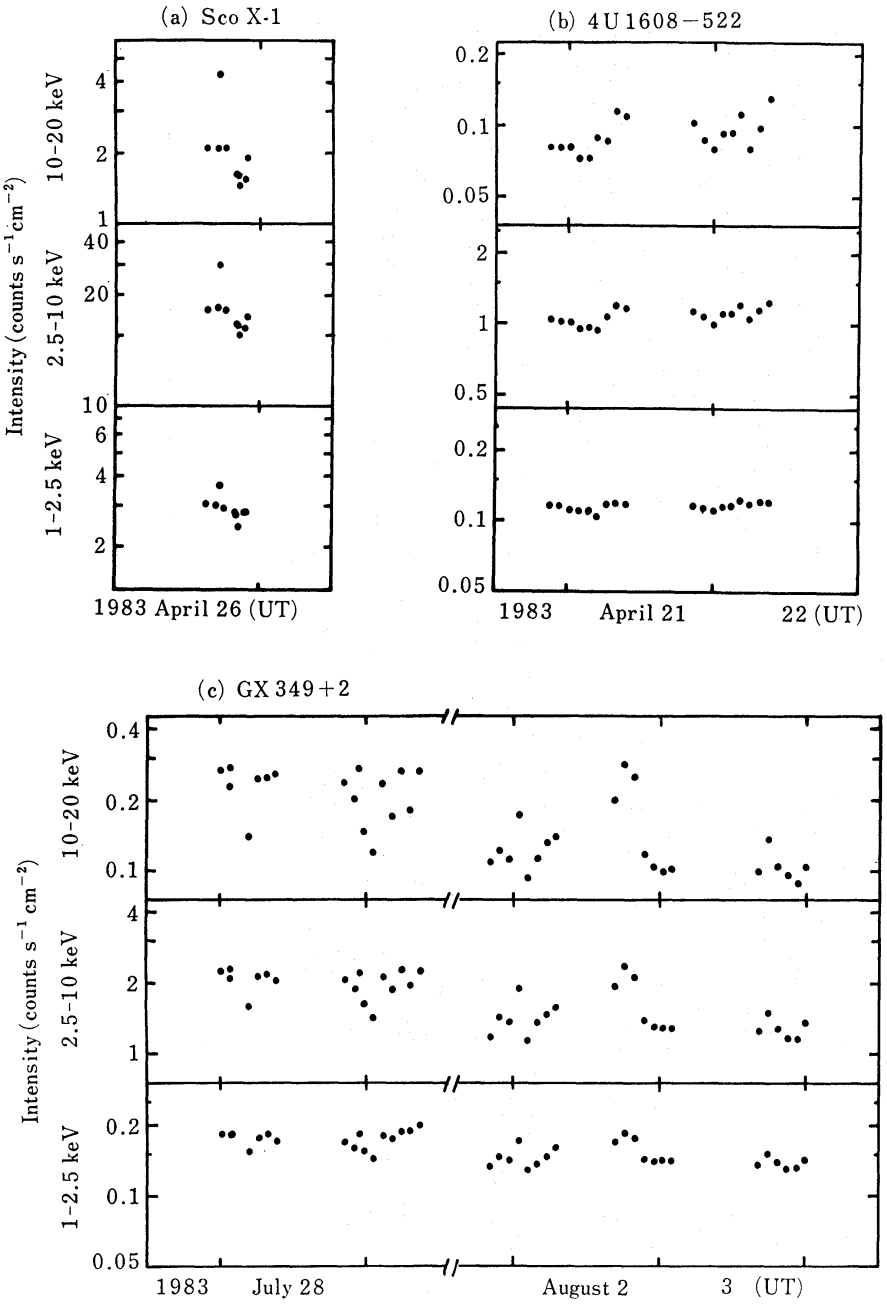

Fig. 1a–c. See the legend on the next page.

of the four sources.

The intensities of the four sources are plotted in figure 1 for three different energy bands, 1–2.5 keV, 2.5–10 keV, and 10–20 keV, as functions of time. Each data point represents average of 10 to 30 min of observation. The transient X-ray source 4U 1608−522 was persistently bright throughout the present observation. Large intensity variations up to a factor of two on time scales of several tens of minute were observed from all the sources. Besides, we detected rapid intensity drops from GX 5−1 (hereafter called dips), during the phase in which the average intensity was relatively low. The times of these dips are indicated by arrows in figure 1.

In general, one notices in figure 1 that the intensity in the lower energy band varies less

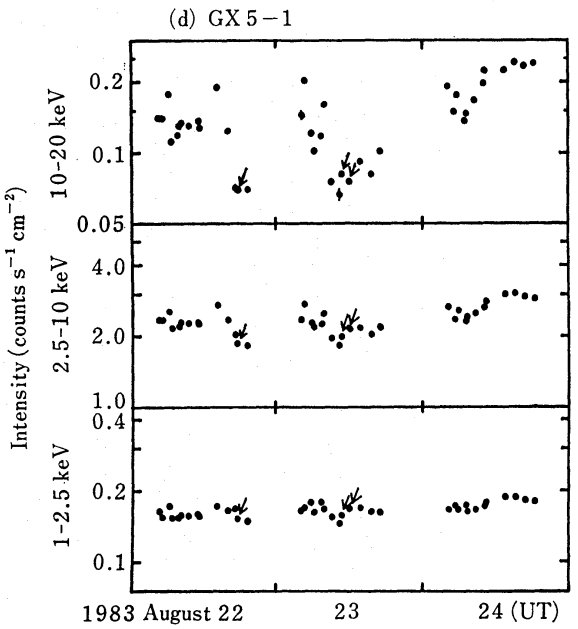

Fig. 1. X-ray intensities in three energy bands, 1–2.5 keV, 2.5–10 keV, and 10–20 keV, as a function of time. Each data point is the average of a continuous data train of 10–30-min length. For most of the data points, the 1σ statistical errors are smaller than the size of symbol. In the three data trains marked by arrows, several intensity dips were observed from GX 5−1.

than that in the higher energy band. Consequently, the spectrum hardens as the total intensity increases.

3. Analysis and Results

Pulse-height spectrum for each 10–30-min observation, corresponding to each data point in figure 1, was obtained for the four sources. No simple model spectrum such as a blackbody, thermal bremsstrahlung or power-law type is found to fit the observed spectra. On the other hand, as shown below, these spectra seem to possess intrinsic characteristics which are common to all the four sources.

3.1. Variation of Spectrum

Each source shows significant variation of spectrum with time. In order to find the property of the spectral variation, we picked up pairs of data points in figure 1, for which the intensities in the range 10–20 keV are different by more than 30%. Each pair of data points was chosen from a period in which no attitude correction of the satellite was executed (typically within a few hours), so as to minimize possible systematic errors in the exposure correction caused by an uncertainty of the collimator response function. In this way, we chose 3 pairs for Sco X-1, 3 pairs for 4U 1608−522, 4 pairs for GX 349+2, and 3 pairs for GX 5−1, respectively.

Figure 2a shows, for example, two pulse-height spectra of one of the pairs for Sco X-1. The ratio of these two spectra is shown in figure 2b. Figure 2b suggests that the flux ratio tends to unity towards lower energies. Towards higher energies, the ratio increases with energy up to 10 keV, whereas it remains constant above 10 keV. This means that, despite a large intensity difference, the shape of the two spectra above 10 keV is the same

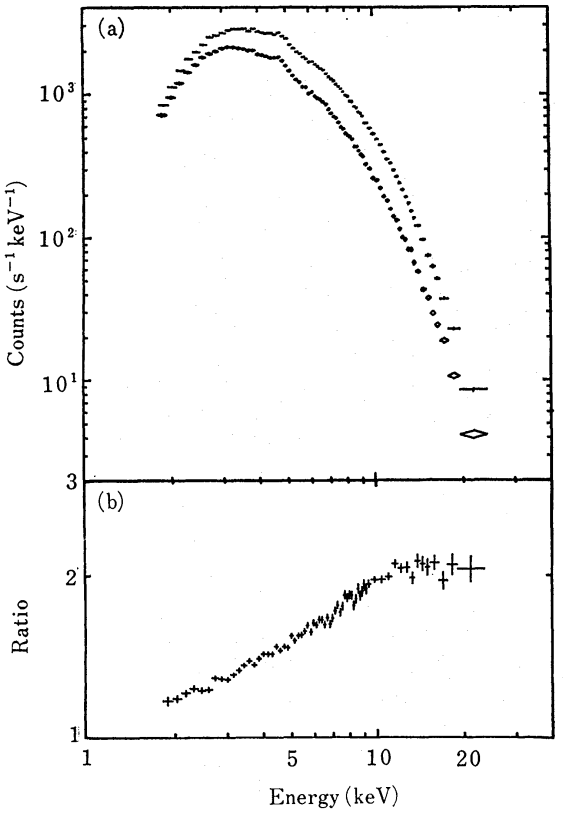

Fig. 2. (a) Two pulse-height spectra of one of the paris for Sco X-1 . They were observed with an interval of about 60 min.
(b) The flux ratio as a function of energy for the two spectra in figure 2a.

within statistical uncertainties. Hence the difference of the two spectra above 10 keV will have the same shape as well. The difference of the two spectra is shown in figure 3. We performed spectral fittings of the difference with three models; power-law, thermal bremsstrahlung, and blackbody spectra. Each model has three free parameters including the absorbing neutral hydrogen column $N_{\rm H}$. The reduced χ^2 values for the best fit in the range 2–15 keV are 49.7 for the power-law spectrum, 27.0 for the thermal bremsstrahlung spectrum, and 1.26 for the blackbody spectrum, for 31 degrees of freedom. Therefore, the differenece spectrum is very well expressed by a blackbody spectrum with kT of 2.06 ± 0.03 keV in the range 2–15 keV. The best-fit blackbody spectrum is shown by the histogram in figure 3a. One notices the presence of a high-energy tail above 15 keV, an excess flux over the blackbody spectrum. The remaining two pairs for Sco X-1 yield a similar result in that only a blackbody spectrum gives a satisfactory fit to the difference spectra, with the best-fit kT values of 1.97 ± 0.05 keV and 1.96 ± 0.07 keV, respectively. Thus, all the three difference spectra have the same kT values, though they differ in intensity. The best-fit kT value for the sum of the three difference spectra of Sco X-1 is determined to be 2.00 ± 0.03 keV.

The same analysis was performed for the pairs of three other sources. Each of the difference spectrum is χ^2-tested for fit with the three model spectra as in the case of Sco X-1. It is again found that only a blackbody spectrum gives a satisfactory fit to each of the observed difference spectrum. The best-fit parameter values of the blackbody spectra together with χ^2 values are given in table 2a. kT values for the pairs from each source are also found to be the same within the errors. The best-fit kT values for the individual sources are 2.11 ± 0.03 keV for 4U 1608−522, 2.12 ± 0.03 keV for GX 349+2, and 1.97 ± 0.05 keV

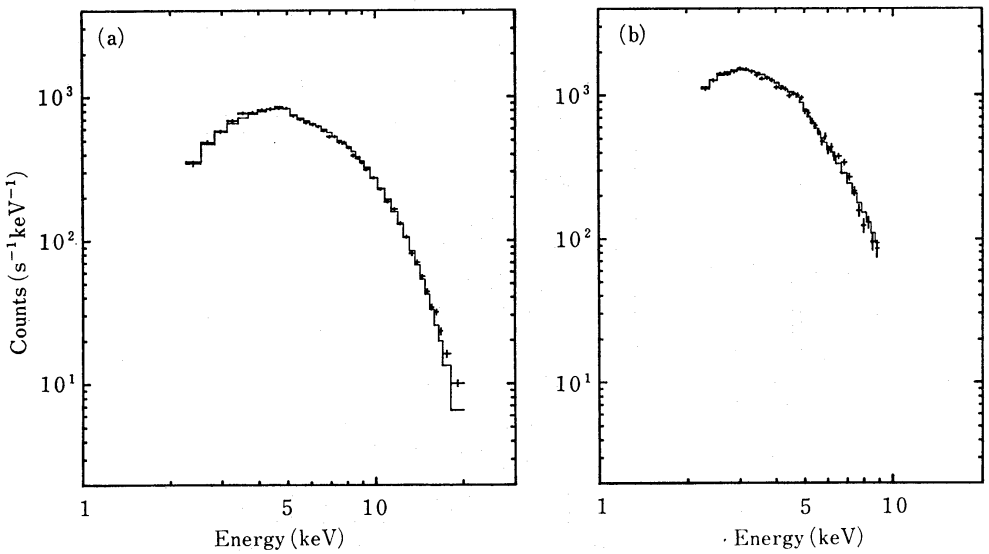

Fig. 3. (a) The difference of the two spectra of Sco X-1 shown in figure 2a. The best-fit blackbody spectrum convolved with the counter response function is shown by the histogram.
(b) The soft component of Sco X-1 derived from the pair in figure 2a. The histogram shows the best-fit "multicolor" spectrum convolved with the counter response function.

for GX 5−1. The kT values are strikingly similar for the four different sources.

3.2. *Decomposition of Spectrum*

The above results show that, at least for the pairs of different intensities chosen for each source, the difference of the spectra always exhibits a blackbody spectrum of $kT\cong 2$ keV and that the shape of each observed spectrum above 10 keV is in good agreement with that of a 2-keV blackbody spectrum (i.e. constant flux ratio above 10 keV as shown in figure 2b). These facts lead us to a hypothesis that the observed spectrum is a sum of two spectral components, a 2-keV blackbody component and a certain softer component. The 2-keV blackbody component changes with time whereas the softer component remains fairly constant. Hereafter, we call the 2-keV blackbody component the hard component and the softer component simply the soft component.

For this hypothesis, an observed spectrum $f(E)$ can be expressed by

$$f(E)=f_{\rm s}(E)+f_{\rm h}(E)\,, \tag{1}$$

where $f_{\rm h}(E)$ and $f_{\rm s}(E)$ are the hard component spectrum and the soft component spectrum, respectively.

Let us suppose the hard componet increased by a factor β. Then,

$$f_{\rm h}(E)=\frac{1}{\beta-1}\left[f_2(E)-f_1(E)\right], \tag{2}$$

$$f_{\rm s}(E)=\frac{1}{\beta-1}\left[\beta f_1(E)-f_2(E)\right], \tag{3}$$

where $f_1(E)$ and $f_2(E)$ are the spectra before and after the increase. Thus, $f_{\rm h}(E)$ is obtained from the difference of the two spectra as shown in the last subsection. $f_{\rm s}(E)$ can be derived

Table 2. Results of spectral fits.

(a) Difference spectra (2–15 keV)

Source	Pair	Blackbody model			
		Bolometric flux* (10^{-8} erg s^{-1} cm^{-2})	Temperature (keV)	N_H (10^{22} cm^{-2})	Reduced χ^2 (d.o.f.=31)
Sco X-1	1	40.9 ±0.6 19.9 ±0.3	2.06±0.03	<0.6	1.26
Sco X-1	2	22.5 ±0.7 17.1 ±0.5	1.97±0.05	<2.	1.00
Sco X-1	3	11.5 ±0.7 8.6 ±0.5	1.96±0.07	<4.	1.26
4U 1608−522	1	1.02±0.07 0.79±0.05	2.12±0.07	3. ±2.	0.88
4U 1608−522	2	0.89±0.05 0.69±0.03	2.07±0.06	<2.	1.08
4U 1608−522	3	0.87±0.05 0.61±0.03	2.11±0.07	3. ±2.	1.17
GX 5−1	1	2.3 ±0.2 1.4 ±0.1	1.96±0.08	4. ±2.	1.61
GX 5−1	2	2.0 ±0.1 0.94±0.07	1.94±0.07	7. ±2.	1.34
GX 5−1	3	0.99±0.04 0.62±0.03	2.0 ±0.1	<8.	1.37
GX 349+2	1	1.8 ±0.1 1.01±0.06	2.1 ±0.1	<4.	0.71
GX 349+2	2	3.32±0.06 1.80±0.03	2.04±0.05	<2.	1.21
GX 349+2	3	3.0 ±0.1 2.2 ±0.1	2.12±0.06	3. ±2.	1.26
GX 349+2	4	2.25±0.03 1.09±0.02	2.11±0.06	<2.	0.72

* Two bolometric flux values for each pair are those of the difference spectrum multiplied by $\beta/(\beta-1)$ and $1/(\beta-1)$ respectively, which correspond to the bolometric fluxes of the two spectra (see text).

Errors quoted are 90% confidence limit.

(b) Decomposed soft components (2–10 keV)

Source	Pair	Blackbody model				"Multicolor" model			
		Bolometric flux (10^{-8} erg s^{-1} cm^{-2})	Temperature (keV)	N_H (10^{22} cm^{-2})	Reduced χ^2 (d.o.f. =30)	Bolometric flux (10^{-8} erg s^{-1} cm^{-2})	T_{in} (keV)	N_H (10^{22} cm^{-2})	Reduced χ^2 (d.o.f. =30)
Sco X-1	1	16.6 ±0.8	1.01±0.02	<1.	3.73	26. ±3.	1.49±0.06	<1.4	1.31
Sco X-1	2	15.3 ±0.4	0.89±0.02	<1.	2.37	23. ±4.	1.27±0.08	<1.4	1.28
Sco X-1	3	15. ±1.	0.91±0.05	<1.	2.09	22. ±6.	1.4 ±0.2	<2.	1.53
4U 1608−522	1	0.86±0.05	0.95±0.03	<1.	1.68	1.3±0.3	1.4 ±0.1	<2.	1.06
4U 1608−522	2	0.74±0.05	0.93±0.03	<1.	1.62	1.2±0.2	1.26±0.09	1.5±0.7	1.55
4U 1608−522	3	0.82±0.03	0.94±0.03	<1.	1.24	1.4±0.2	1.26±0.08	2.0±0.8	0.76
GX 5−1	1	2.5 ±0.4	1.04±0.06	3. ±1.	1.35	3.5±0.9	1.4 ±0.1	3.5±1.2	1.06
GX 5−1	2	2.6 ±0.2	1.03±0.05	2. ±1.	1.77	4.5±0.6	1.36±0.06	4.6±0.8	1.36
GX 5−1	3	2.1 ±0.2	1.04±0.08	<3.	0.89	4.7±1.0	1.3 ±0.1	6.6±1.2	1.22
GX 349+2	1	1.0 ±0.1	1.04±0.06	<1.	0.99	1.8±0.5	1.5 ±0.2	<2.3	0.71
GX 349+2	2	0.86±0.06	0.97±0.04	<1.	1.60	1.5±0.2	1.3 ±0.1	<2.	1.49
GX 349+2	3	1.2 ±0.1	1.01±0.05	<1.	1.09	1.8±0.3	1.5 ±0.2	1.5±0.9	0.99
GX 349+2	4	0.90±0.04	0.99±0.03	<1.	1.57	1.5±0.2	1.4 ±0.1	1.5±0.7	1.17

Errors quoted are for 90% confidence limit.

(c) Dip of GX 5−1 (2–15 keV)

	Blackbody model				"Multicolor" model			
	Bolometric flux (10^{-8} erg s^{-1} cm^{-2})	Temperature (keV)	N_H (10^{22} cm^{-2})	Reduced χ^2 (d.o.f. =59)	Bolometric flux (10^{-8} erg s^{-1} cm^{-2})	T_{in} (keV)	N_H (10^{22} cm^{-2})	Reduced χ^2 (d.o.f. =59)
Dip 1	2.2±0.1	1.22±0.02	<1.	2.44	3.8±0.2	1.59±0.03	3.7±0.4	1.47
Dip 2	2.2±0.1	1.21±0.03	<1.	1.83	3.7±0.3	1.60±0.05	3.7±0.5	1.17
Dip 3	2.3±0.1	1.19±0.02	<1.	3.06	4.0±0.2	1.56±0.03	4.1±0.4	1.19

Quoted errors are for 90% confidence limit.

(d) Difference between pre-/post-dip and dip spectra (2–15 keV)

	Blackbody model			
	Bolometric flux (10^{-8} erg s^{-1} cm^{-2})	Temperature (keV)	N_H (10^{22} cm^{-2})	Reduced χ^2 (d.o.f=24)
Dip 1	0.36±0.09	1.9±0.2	<8.	1.23
Dip 2	0.40±0.05	1.8±0.1	<8.	1.24
Dip 3	0.41±0.05	1.7±0.1	<8.	1.19

Quoted errors are for 90% confidence limit.

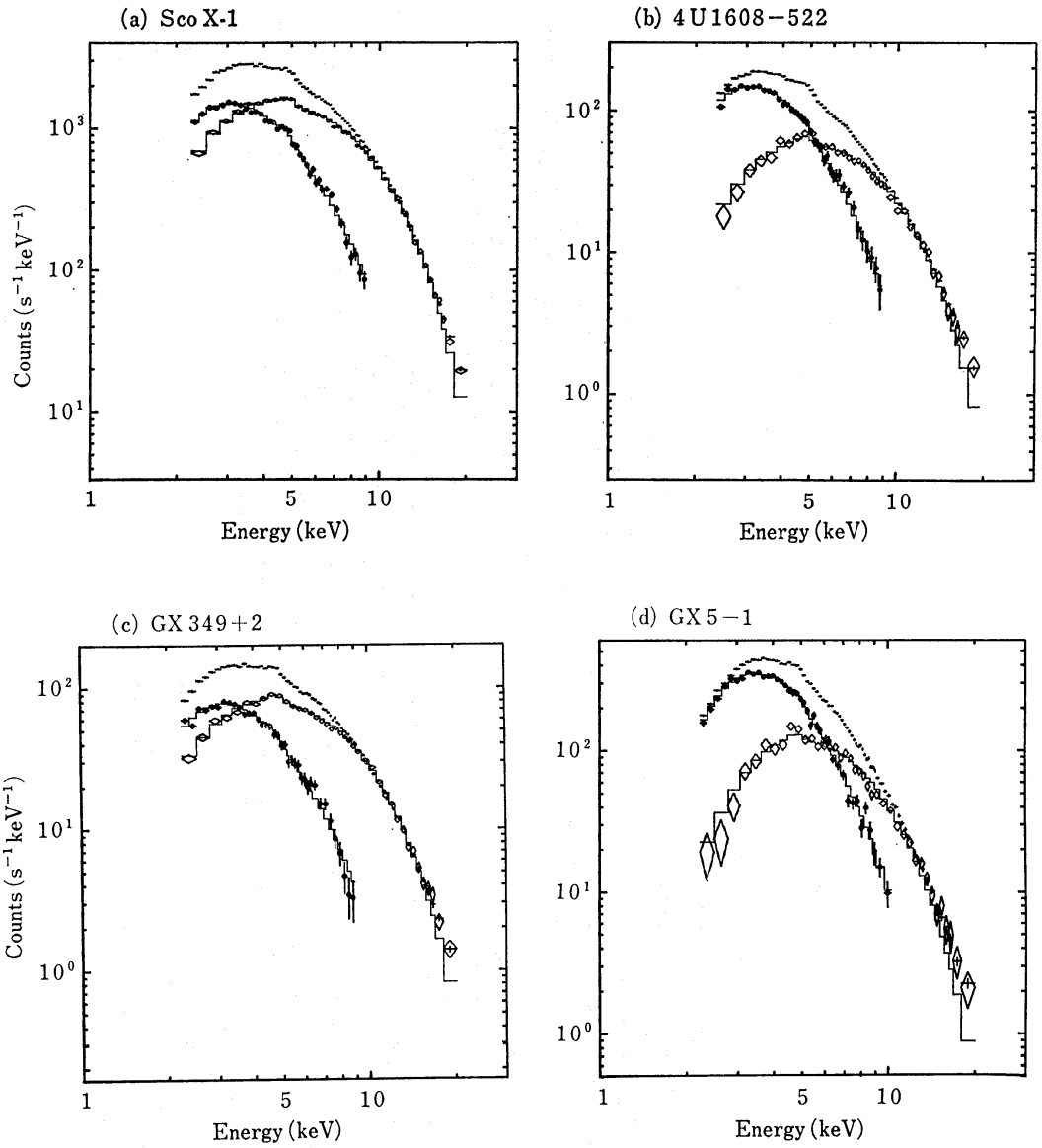

Fig. 4. Examples of the spectrum in the pairs for Sco X-1, 4U 1608−522, GX 349+2, and GX 5−1 (cross), and the decomposed soft (crossed circle) and hard components (rhomb). The best-fit model spectra of the two components are shown by the histograms.

as the difference between the two spectra after normalizing $f_1(E)$ to $f_2(E)$ in the range above 10 keV. Figure 3b shows $f_s(E)$ so-obtained for the pair of Sco X-1 spectra shown in figure 2a.

The same procedure was applied to the remaining 12 pairs of spectra to derive $f_s(E)$ for each pair. For the resultant spectra, we tested four different models, power-law spectrum, thermal bremsstrahlung spectrum, blackbody spectrum, and the spectrum expected from an optically thick accretion disk. The last one is a superposition of blackbody spectra according to a certain temperature distribution as described in section 4, which we shall call the "multicolor" spectrum. Each model has three free parameters including N_H. Power-law and thermal bremsstrahlung spectra resulted in χ^2 values which were too large to be acceptable. The result of the fittings with blackbody spectrum and the "multicolor"

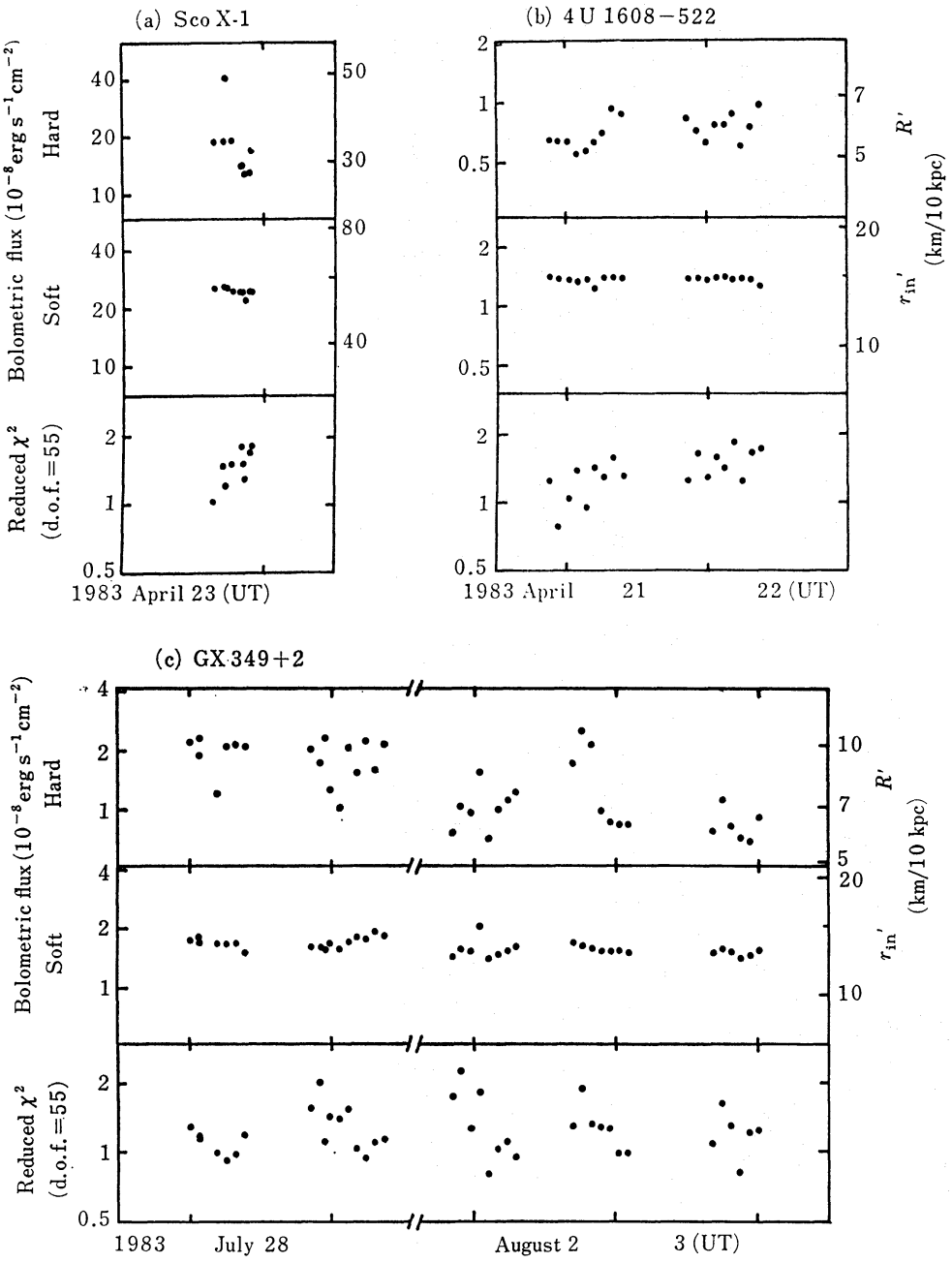

Fig. 5a, b, and c. See the legend on the next page.

spectrum is summarized in table 2b. As seen in the table, the "multicolor" spectrum is always found to be acceptable for 99% confidence level. Blackbody spectrum gives poorer fit than the "multicolor" spectrum, though in several cases the χ^2 value is within an acceptable range. Blackbody spectrum is however considered to be unlikely as discussed in section 4. Figures 4a–d show examples of the observed spectra for Sco X-1, 4U 1608−522, GX 349+2, and GX 5−1 and the decomposed hard and soft components, respectively. The best-fit 2-keV blackbody and the "multicolor" spectra are also shown by histograms in the same figures.

For each individual source, the shape of the soft component among the pairs is found consistent to be the same within the errors. The weighted mean of the soft component is

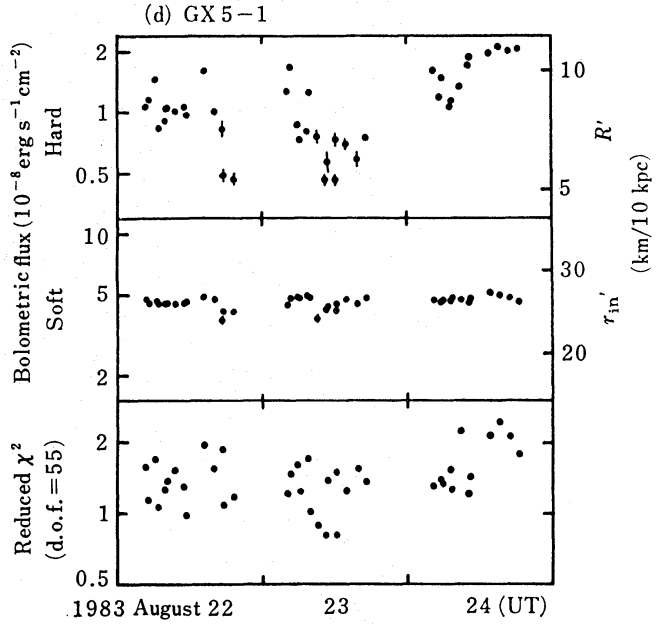

Fig. 5. The results of the spectral fitting by a combination of the blackbody and the "multicolor" spectra. Two free parameters, the bolometric fluxes of the soft and hard components, and the reduced χ^2 values are plotted against time. In the fits, the shape of the both components and the value of N_H are fixed to those values obtained from the average spectra of both components obtained from the pairs for each source, except for a few data points of GX 5−1, where a slightly lower temperature of the blackbody is used (see text).

obtained for each source and the best-fit parameters for the "multicolor" spectrum are determined. The values of the parameter kT_{in} (see section 4) which determines the shape of the "multicolor" spectrum are 1.38 ± 0.06 keV for Sco X-1, 1.30 ± 0.06 keV for 4U 1608−52, 1.44 ± 0.08 keV for GX 349+2, and 1.36 ± 0.06 keV for GX 5−1, respectively. It is remarkable that the kT_{in} values are about the same for the four different sources.

As a next step for testing of the two-component hypothesis, we examined whether or not every observed spectrum can be explained by a combination of the best-fit 2-keV blackbody and the "multicolor" spectra for each source as determined above. In this case, the free parameters are only two; the total intensities of the two spectral components. The fitting was performed in the range 2–5.7 and 7.7–15 keV for 55 degrees of freedom. We omitted the energy range 5.7–7.7 keV in order to avoid the influence of the weak iron emission line, which is treated in a separate paper (Suzuki et al. 1984). For a few spectra of GX 5−1, a slightly lower blackbody temperature was used as discussed in the next subsection. The result is shown in figure 5, in which the best-fit bolometric fluxes of the 2-keV blackbody and accretion disk components are plotted for each observation together with respective χ^2 values. The fit is found to be satisfactory for most of the observed spectra. In the cases of relatively large χ^2 values (the largest being 2.4 for the reduced χ^2), the deviation is mostly due to an excess flux over the 2-keV blackbody spectrum above 10 keV. It is clearly seen in figure 5 that the intensity of the soft component remains fairly constant with time.

3.3. *Intensity Dips of GX 5−1*

During the observation of GX 5−1, several intensity dips were recorded. The light curves including these dips are shown in figure 6. These dips are characterized by the rise and fall in a few tens of second and a duration of the order of one minute. All the observed

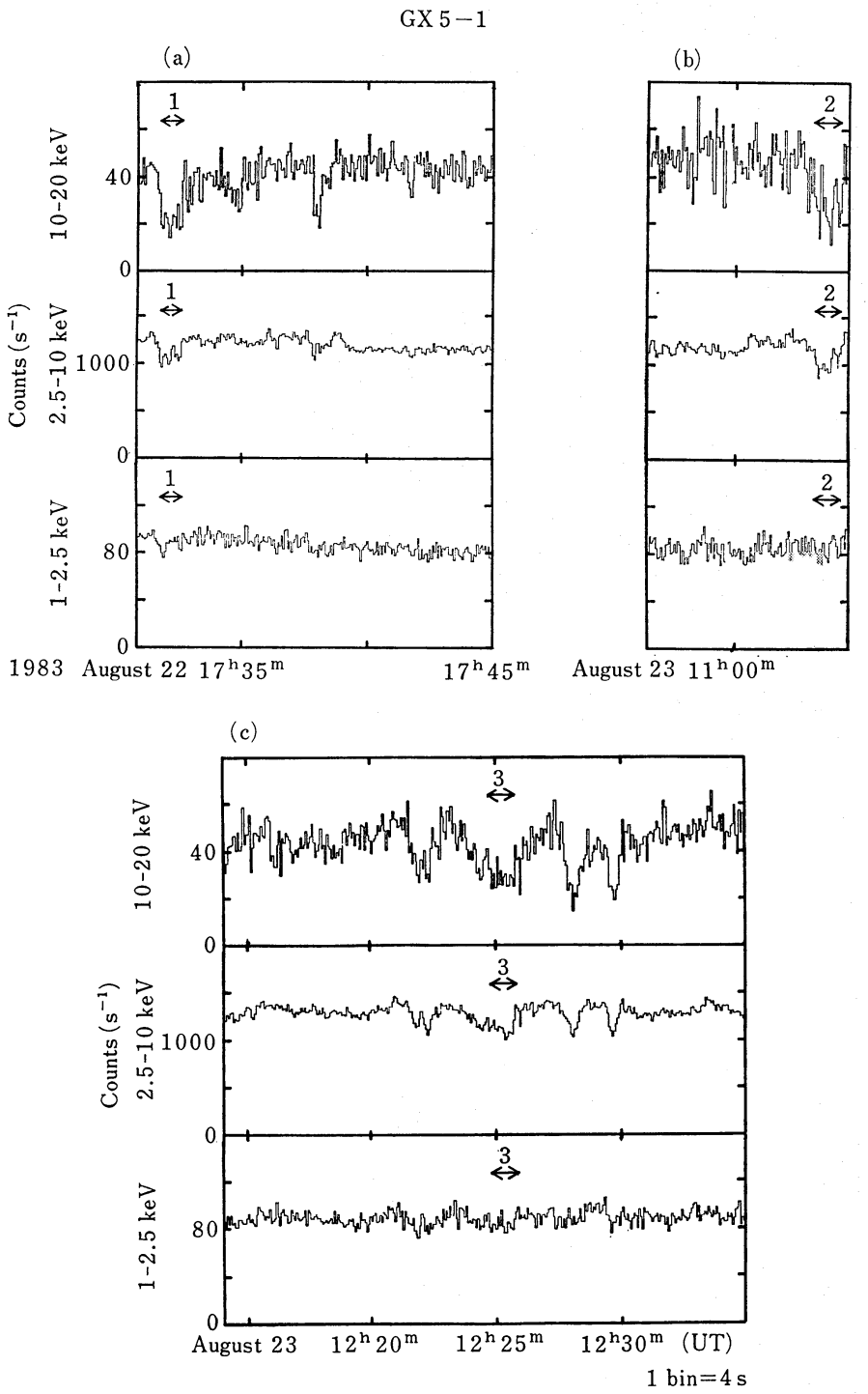

Fig. 6. Count rate of GX 5−1 as a function of time in three energy bands, 1–2.5 keV, 2.5–10 keV, and 10–20 keV, for three data trains where intensity dips were detected. The count rate is for an effective area of 640 cm² after the background subtraction and the aspect correction. The small periodic variation with a period of about 30 s is instrumental and should be ignored.

dips occurred when the average intensity was around the minimum level.

We examined the spectra of those three dips that are indicated in figure 6. Figure 7

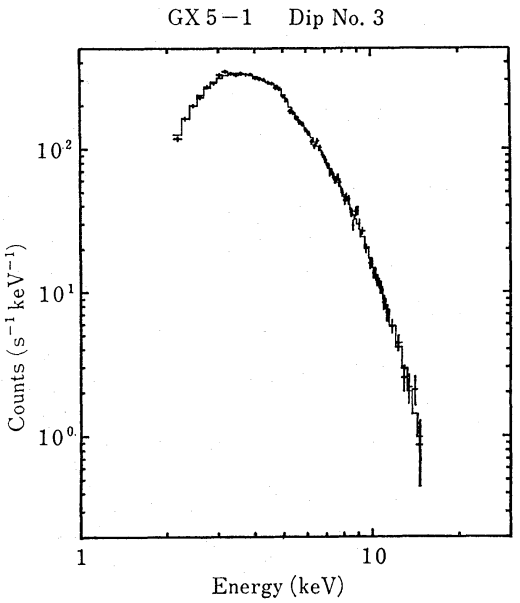

Fig. 7. Pulse-height spectrum during a dip (dip 3 in figure 6). The histogram shows the best-fit "multicolor" spectrum convolved with the counter response function. Note the close similarity to the soft component of GX 5−1 shown in figure 4d.

shows an example of the pulse-height spectrum during one of the dips (dip No. 3). For the spectral fittings, four models were employed; power-law, thermal bremsstrahlung, blackbody, and the "multicolor" spectra, respectively. It is found that only the "multicolor" spectrum can satisfactorily reproduce the observed dip spectra. The best-fit parameter values are listed in table 2c. It is to be noted that the observed spectra during the dips are in agreement with each other. The $kT_{\rm in}$ values for the dips appear to be slightly higher than that for the decomposed soft component. One might suspect that this is due to a small contribution of the hard component. However, the two-component fittings to the dip spectra, with inclusion of a hard component as performed in the last subsection, did not improve the fit. Based on the hypothesis of the two spectral components, the dip can be explained as the case in which the hard component has become almost totally absent and we observe the stable soft component alone.

If one subtracts the dip spectrum from that observed in the neighboring period, the difference is again well expressed by a blackbody spectrum. The best-fit parameter values are given in table 2d. However, the best-fit blackbody temperature appears to be slightly lower than those determined previously from the pairs (table 2a). These pairs happen to be taken from the period when the average intensity level was significantly higher than that seen in the neighborhood of the dips. In other words, the relative intensity of the blackbody component is much smaller in the latter period. This fact may have to do with the lower blackbody temperature. In fact, the observed spectra of GX 5−1 near the minimum intensity level are satisfactorily reproduced by the two components, if the lower blackbody temperature is employed.

4. Discussion

It is shown in the preceding section that two fixed spectral components, the 2-keV blackbody component and the "multicolor" component, are necessary and sufficient to express all observed spectra from each individual source. Furthermore, the key parameter values for the two components, the blackbody temperature and the innermost disk temperature (see below), are nearly the same among the four sources. We consider that this is a common and intrinsic characteristics of the nonpulsating low-mass binary sources involving a neutron star. An important feature is that the intensity of the hard (2-keV blackbody) component can change largely while the soft (multicolor) component remains stable. This fact strongly suggests different origins for the two components. In what follows, we shall consider the observed result in the context of the accretion disk model of the neutron star.

In the nonpulsating low-mass binary sources, the magnetic field of the neutron star is considered to be so weak that it will not influence the accretion flow. Hence, the accretion disk will extend to the neutron star surface. When the matter circulating along the Keplerian orbit gradually falls inward, half the gravitational energy released will be converted to thermal energy in the accretion disk, whereas another half will be carried over to the neutron star in the form of kinetic energy of the accreting matter. Since the angular velocity of the surface is much smaller than that of the matter in Keplerian motion, the accreting matter should release its kinetic energy on the neutron star surface as it settles down. One would therefore expect two separate emission regions; the accretion disk and the neutron star surface. It is natural to consider that the observed two spectral components may be related to these two emission regions. Interpretation of the energy spectra of low-mass binary sources in terms of the emission from these two regions has been proposed by Shibazaki and Mitsuda (1984), Hayakawa et al. (1984), and Hirano et al. (1984). We shall examine the properties of emission from the two regions.

The structure of the accretion disk around the neutron star, when the effect of magnetic field is negligible, was recently discussed in detail by Hoshi (1984 b, see also the references therein). According to this model, the accretion disk outside a certain radius will be optically thick, and the energy released in this region will be radiated as blackbody emission from the surface of the accretion disk. Whereas, the inner part of the disk, where the radiation pressure is dominant, is considered to be inflated and will become optically thin. The energy released inside this region cannot be radiated efficiently due to low gas density and will be converted to the internal energy which is eventually transported to the neutron star. This energy and the kinetic energy of the Keplerian motion will be radiated as blackbody emission from the neutron star atmosphere which is considered to be optically thick. Therefore, if one denotes the luminosity of the optically thick disk and that of the neutron star surface by $L_{\rm d}$ and $L_{\rm b}$, respectively, it will generally follow that $L_{\rm b} \geq L_{\rm d}$.

In an optically thick disk, the energy radiated from the disk between r and $r-\Delta r$, $4\pi r \Delta r \sigma T^4$, is equal to the energy released in Δr which is proportional to $r^{-2}\Delta r$. Therefore, T will depend on r as $r^{-3/4}$. The observed spectrum from the optically thick disk $f_{\rm d}(E)$ for an inclination with respect to the line of sight θ and at a distance D is given by

$$f_{\rm d}(E)=\frac{\cos\theta}{D^2}\int_{r_{\rm in}}^{r_{\rm out}} 2\pi r B(E,T)dr=\frac{8\pi r_{\rm in}^2\cos\theta}{3D^2}\int_{T_{\rm out}}^{T_{\rm in}}\left(\frac{T}{T_{\rm in}}\right)^{-11/3} B(E,T)\frac{dT}{T_{\rm in}}, \quad (4)$$

where $r_{\rm in}$ and $r_{\rm out}$ are respectively the inner and outer boundaries of the optically thick disk, $B(E, T)$ the Planckian distribution, $T_{\rm in}=T(r_{\rm in})$ and $T_{\rm out}=T(r_{\rm out})$, respectively. This

is the "multicolor" spectrum that has been used for the spectral fittings in the last section. The luminosity of the optically thick disk L_d is obtained by

$$L_d=\int_{r_{in}}^{r_{out}} 4\pi r\sigma T^4(r)dr\cong 4\pi {r_{in}}^2\sigma {T_{in}}^4 . \quad (5)$$

The last expression holds for $r_{out}\gg r_{in}$.

On the other hand, the observed spectrum from the neutron star surface $f_b(E)$ is expressed for a blackbody temperature T_b by

$$f_b(E)=\frac{S'}{D^2}B(E, T_b) , \quad (6)$$

where S' denotes the projected area of the emitting region to the plane perpendicular to the line of sight. The corresponding luminosity L_b is given by

$$L_b=S\sigma {T_b}^4, \quad (7)$$

for the total area of the emitting region S on the neutron star surface. Since S is a certain fraction of the whole surface of the neutron star, $S<4\pi R^2$ with R being the neutron star radius. It then follows generally that $T_b>T_{in}$ from equations (5) and (7) combined with the relations $r_{in}>R$ and $L_b\geq L_d$.

From the above result, it is very plausible to interpret that the observed soft component is the emission from the optically thick accretion disk and the hard component corresponds to the emission from the neutron star surface. In fact, in last section, the "multicolor" spectrum given by equation (4) is shown to best fit the observed soft components. Some of the observed soft components gave an acceptable fit to a blackbody spectrum of $kT\sim 1$ keV. However, the observed spectrum of Sco X-1 (Deerenberg et al. 1973; Kahn et al. 1981) shows an intense flux even in the range below 1 keV, which is incompatible with this blackbody spectrum. We may therefore exclude the blackbody spectrum for the soft component.

In figure 5 are also given the two quantities (right-hand scale), $R'=(S'/\pi)^{1/2}$ and $r_{in}'=r_{in}(\cos\theta)^{1/2}$, which are derived from the two-component fittings of each observed spectrum by using equations (4) and (6). The distance D is fixed to be 10 kpc. While the inclination angle θ is unknown, the observed results always satisfy the relation $r_{in}'>R'$, which is at least consistent with the present interpretation.

The flux of the hard component varies widely for all the sources. Since the blackbody temperature is found to remain constant, it implies that the emitting area on the neutron star surface changes with flux. This may be understood in terms of the local Eddington limit. If the radiation flux per unit area of the emitting neutron star surface reached the Eddington limit, the temperature can no more increase. For more energy to radiate, the surface area of emission will have to increase. The maximum temperature corresponding to the Eddington limit is determined by the local gravity field (Marshall 1982). In fact, the observed temperature ~ 2 keV is a little in excess of the maximum temperature expected for a $1.4M_\odot$ neutron star. This may be explained by the difference between the effective temperature and the color temperature (Hoshi 1984a), of which the latter is the one determined from the observed spectrum.

Most of the observed spectra show an excess flux over the blackbody spectrum above 15 keV for all the four sources. This deviation may be an indication of the presence of a hard tail which was reported for Sco X-1 and GX 349+2 [see references in Miyamoto and Matsuoka (1977); Greenhill et al. (1979)]. The presence of a hard tail is expected from the accretion disk model as a result of the Comptonization of the blackbody photons from

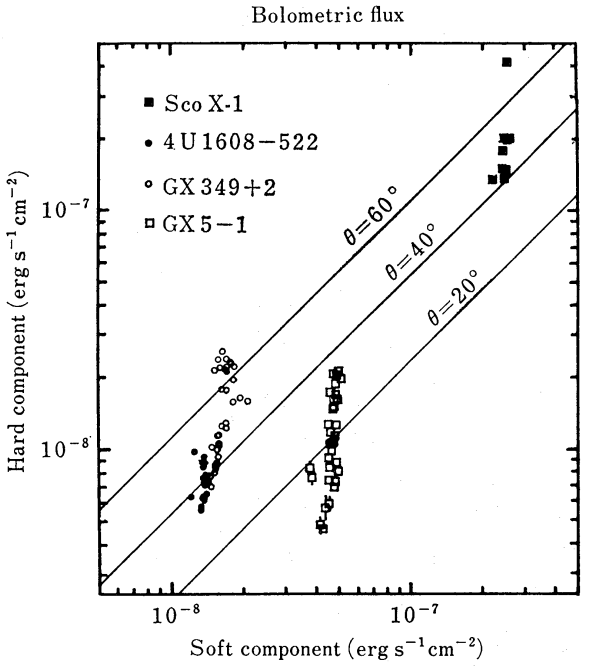

Fig. 8. Bolometric flux of the hard component versus that of the soft component, derived from the two-component spectral fits (figure 5). Three lines show the loci of $L_b=L_d$ for the inclination angles of 20°, 40°, and 60°, where the emission region of the hard component is assumed to be a narrow equatorial zone of the neutron star surface.

the neutron star surface through the optically thin region of the inner disk ($r<r_{in}$) (Hoshi 1984b).

As regards the soft component, the derived accretion disk parameters T_{in} and r_{in}' are found to be remarkably constant in spite of large changes of the hard component. This fact would imply that the accretion flow itself down to r_{in} is kept fairly constant with time. Whereas, the flow inside r_{in} may be variable to cause large changes of the hard component. In particular, the dips observed from GX 5−1 may be demonstrating that the flow onto the neutron star can stop or start within a short time of the order of 10 s. This suggests the presence of some instability in the flow inside r_{in}.

Figure 8 shows the relation between the observed bolometric fluxes of the soft component F_s and the hard component F_h. The data points shown in figure 5 are plotted in this diagram. In the present interpretation of the two components, the ratio of the average bolometric fluxes $\bar{F}_h/\bar{F}_s$ is dependent on the inclination angle of the accretion disk. If the hard component is emitted from the equatorial zone of the neutron star where the accretion disk contacts the surface, the ratio is approximately given from the equations (4) and (6) by

$$\bar{F}_h/\bar{F}_s \cong \frac{2}{\pi} \tan\theta \frac{L_b}{L_d} . \qquad (8)$$

The lines in figure 8 indicate the expected ratios for different inclination angles in the limit $L_b=L_d$. The ratio for GX 5−1 is significantly smaller than those for the other sources. Probably, we are looking at the accretion disk of GX 5−1 near face-on so that the projected area of the equatorial zone is small.

5. Summary

(1) The present result shows that the observed energy spectra of the four low-mass binary X-ray sources can always be expressed by a sum of two fixed spectral components: a hard component with a blackbody spectrum of $kT \cong 2$ keV and a soft component with the "multicolor" spectrum expected from an optically-thick accretion disk.

(2) In terms of the accretion disk model, the hard component can be interpreted as the emission from the neutron star surface, and the soft component as the emission from the optically-thick accretion disk.

(3) The result implies that the accretion flow within the optically-thick disk is stable, whereas the flow onto the neutron star surface is highly variable and can stop occasionally as the dips of GX 5−1.

One of the authors (K.K.) is grateful to Dr. J. Swank, NASA/Goddard Space Flight Center, for valuable discussions on the spectra of the low mass binary X-ray sources.

References

Branduardi, G., Kylafis, N. D., Lamb., D. Q., and Mason, K. O. 1980, *Astrophys. J. Letters*, **253**, L153.

Chapline, G. Jr., and Stevens, J. 1973, *Astrophys. J.*, **184**, 1041.

Deerenberg, A. J. M., Bleeker, J. A. M., de Korte, P. A. J., Yamashita, K., Tanaka, Y., and Hayakawa, S. 1973, *Nature Phys. Sci.*, **244**, 4.

Felten, J. E., and Rees, M. J. 1972, *Astron. Astrophys.*, **17**, 226.

Greenhill, J. G., Coe, M. J., Bell-Burnell, S. J., Strong, K. T., and Carpenter, G. F. 1979, *Monthly Notices Roy. Astron. Soc.*, **189**, 563.

Hayakawa, S., Hirano, T., Kunieda, H., and Nagase, F. 1984, *Adv. Space Res.*, **3**, Nos. 10–12, 67.

Hirano, E., Hayakawa, S., Kunieda, H., Makino, F., Masai, K., Nagase, F., and Yamashita, K. 1984, *Publ. Astron. Soc. Japan*, **36**, 679.

Hoffman, J. A., Lewin, W. H. G., Primini, F. A., Wheaton, W. A., Swank, J. H., Boldt, E. A., Holt, S. S., Serlemitsos, P. J., Share, G. H., Wood, K., Yentis, D., Evans, W. D., Matteson, J. L., Gruber, D. E., and Peterson, L. E. 1979, *Astrophys. J. Letters*, **233**, L51.

Hoshi, R. 1984a, in *High Energy Transients in Astrophysics, AIP Conference Proceedings No. 115*, ed. S. E. Woosley (American Institute of Physics, New York), p. 325.

Hoshi, R. 1984b, *Publ. Astron. Soc. Japan*, **36**, 785.

Kahn, S. M., Charles, P. A., Bowyer, S., and Blissett, R. J. 1981, *Astrophys. J.*, **250**, 733.

Koyama, K., Ikegami, T., Inoue, H., Kawai, N., Makishima, K., Matsuoka, M., Mitsuda, K., Murakami, T., Ogawara, Y., Ohashi, T., Suzuki, K., Tanaka, Y., Waki, I., and Fenimore, E. E. 1984, *Publ. Astron. Soc. Japan*, **36**, 659.

Lamb, P., and Sanford, P. W. 1979, *Monthly Notices Roy. Astron. Soc.*, **188**, 555.

Laros, J. G., and Singer, S. 1976, *Astrophys. J.*, **205**, 550.

Long, K. S., and Kestenbaum, H. L. 1978, *Astrophys. J.*, **226**, 276.

Marshall, H. L. 1982, *Astrophys. J.*, **260**, 815.

Mason, K. O., Charles, P. A., White, N. E., Culhane, J. L., Sanford, P. W., and Strong, K. T. 1976, *Monthly Notices Roy. Astron. Soc.*, **177**, 513.

Miyamoto, S. 1978, *Astron. Astrophys.*, **63**, 69.

Miyamoto, S., and Matsuoka, M. 1977, *Space Sci. Rev.*, **20**, 687.

Oda, M. 1984, in *High Energy Transients in Astrophysics, AIP Conference Proceedings No. 115*, ed. S. E. Woosley (American Institute of Physics, New York), p. 103.

Parsignault, D. R., and Grindlay, J. E. 1978, *Astrophys. J.*, **225**, 970.

Ponman, T. 1982, *Monthly Notices Roy. Astron. Soc.*, **201**, 769.

Shibazaki, N., and Mitsuda, K. 1984, in *High Energy Transients in Astrophysics, AIP Conference Proceedings No. 115*, ed. S. E. Woosley (American Institute of Physics, New York), p. 63.

Suzuki, K., Matsuoka, M., Inoue, H., Mitsuda, K., Ohashi, T., Tanaka, Y., Hirano, T., and Miyamoto, S. 1984, *Publ. Astron. Soc. Japan,* **36**, 761.

Tanaka, Y., Fujii, M., Inoue, H., Kawai, N., Koyama, K., Maejima, Y., Makino, F., Makishima, K., Matsuoka, M., Mitsuda, K., Murakami, T., Nishimura, J., Oda, M., Ogawara, Y., Ohashi, T., Shibazaki, N., Suzuki, K., Waki, I., Yamagami, T., Kondo, I., Murakami, H., Hayakawa, S., Hirano, T., Kunieda, H., Masai, K., Nagase, F., Sato, N., Tawara, Y., Kitamoto, S., Miyamoto, S., Tsunemi, H., Yamashita, K., and Nakagawa, M. 1984, *Publ. Astron. Soc. Japan,* **36**, 641.

White, N. E., Charles, P. A., and Thorstensen, J. R. 1980, *Monthly Notices Roy. Astron. Soc.*, **193**, 731.